

Highly Fluorescent, Water-Soluble, Size-Tunable Gold Quantum Dots

Jie Zheng, Caiwei Zhang, and Robert M. Dickson*

School of Chemistry and Biochemistry, Georgia Institute of Technology, Atlanta, Georgia 30332-0400, USA

(Received 10 March 2004; published 13 August 2004)

Highly fluorescent, water-soluble, few-atom Au quantum dots have been created that behave as multielectron artificial atoms with discrete, size-tunable electronic transitions throughout the visible and near IR. Correlation of nanodot sizes with emission energies fits the simple relation, $E_{\text{Fermi}}/N^{1/3}$, predicted by the jellium model. Providing the “missing link” between atomic and nanoparticle behavior in noble metals, these emissive, water-soluble Au nanoclusters open new opportunities for biological labels, energy transfer pairs, and light emitting sources in nanoscale optoelectronics.

DOI: 10.1103/PhysRevLett.93.077402

PACS numbers: 78.67.Hc, 36.40.Vz, 73.22.-f, 81.07.Ta

Analogous to the alkali metals, the high electron density, strong electron-electron coupling, and efficient screening [1,2] should make the electronic structure of noble metals change dramatically with nanocluster size and geometry, but the influence of the d electrons is thought to significantly complicate the free-electron behavior [3,4]. Gold exhibits size-tunable plasmon absorption widths by confining conduction electrons in both ground and excited states to dimensions smaller than the electron mean free path (~ 20 nm) [2]. Further confinement of the free electrons, however, reaches a second critical size scale—the Fermi wavelength of an electron (~ 0.7 nm) which should result in discrete, quantum-confined electronic transitions [3]. While such sub-nm nanoclusters are too small to have the continuous density of states (DOS) necessary to support a “plasmon” characteristic of larger free-electron metal nanoparticles [4,5], the jellium model predicts that nanoparticle plasmon widths and nanocluster transition energies of true free-electron metals should both scale with inverse cluster radius. As gas phase photodissociation experiments are unable to probe the lowest energy transitions [4], the size-dependent behavior of noble metals and the development of the plasmon remain poorly understood [1,4,6–9]. While solubilizing and stabilizing organic scaffolds have enabled creation of gold nanoclusters with weak blue and IR emission [6,10] with several reports of plasmon-enhanced emission from larger nanoparticles [11,12] these capping agents limit Au nanocluster size/property determinations. Recently, we were able to utilize well-defined poly(amidoamine) dendrimers (PAMAM) [13] to encapsulate Au_8 nanoclusters exhibiting very clean mass spectra, bright blue emission, and two-order-of-magnitude improved fluorescence quantum yields (42%) in aqueous solution [14]. Here, we report the creation of quantum-confined, water-soluble, high quantum yield Au nanodots with discrete absorption and fluorescence that are size tunable from the UV to the near IR. The discrete absorptions and emissions scale with the number of atoms, N , as $N^{-1/3}$, precisely as predicted by the spherical jellium model, but in contrast to the

$N^{-2/3}$ scaling for semiconductor quantum dots [15] that do not exhibit the free-electron shell-filling degeneracies characteristic of metals. These two cases correspond to multi- and single-electron artificial atoms, respectively. Bridging the gap between discrete gas phase absorptions of analogous alkali metal nanoclusters and the characteristic plasmon absorptions of large noble metal nanoparticles in solution, these few-atom water-soluble Au species offer the “missing link” between atomic and nanoparticle optical properties with clear protoplasmonic fluorescence arising from intraband transitions of the nanocluster free electrons.

Nearly spectrally pure, size-tunable Au nanodots (Fig. 1) are readily synthesized through the slow reduction of gold salts (e.g., HAuCl_4 or AuBr_3) within aqueous PAMAM solutions, followed by centrifugation to remove large nanoparticles. Created through this general procedure [16], differently sized fluorescent gold nanoclusters exhibit discrete excitation and emission spectra from the ultraviolet to the near infrared. Because Au_8 is a magic cluster size, it is usually present to a small degree in each nanodot solution. Both the relative Au:PAMAM concentration and the dendrimer generation [17] enable optimization of the desired nanocluster emission color. These PAMAM-encapsulated nanodots exhibit orders-of-magnitude higher fluorescence quantum yields than do other matrices [6,10] suggesting an important role of amines in Au-nanodot creation.

While nanodot solutions are largely spectrally pure, many nonfluorescent products appear in the mass spectra. Consequently, to determine each fluorescent nanocluster size, fluorescence intensity at each wavelength was correlated with electrospray ionization mass spectrometry abundance for each solution (Fig. 2). In each case, there was a one-to-one correspondence between only one specific peak in the mass spectrum and a specific fluorescent transition to yield linear correlations that enable direct determination of the UV (Au_5), blue (Au_8), green (Au_{13}), red (Au_{23}), and near IR (Au_{31}) emitting species. All aqueous nanodot solutions are very stable, lasting for months either in solution or as dried powders. Solutions

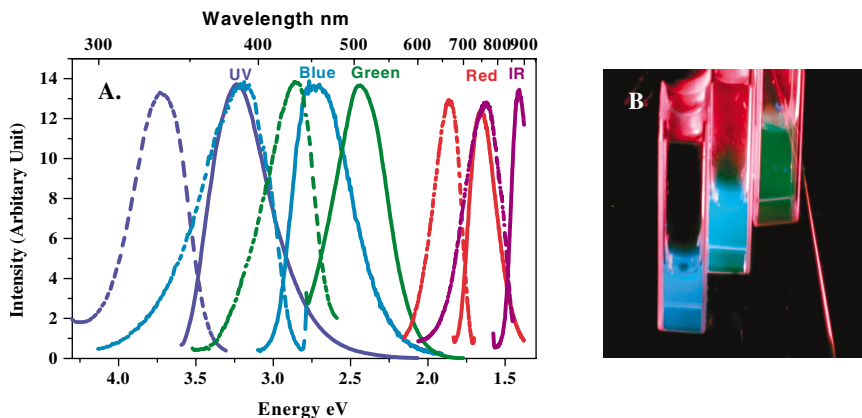


FIG. 1 (color). (a) Excitation (dashed) and emission (solid) spectra of different gold nanoclusters. Emission from the longest wavelength sample was limited by the detector response. Excitation and emission maxima shift to longer wavelength with increasing initial Au concentration [16], suggesting that increasing nanocluster size leads to lower energy emission. (b) Emission from the three shortest wavelength emitting gold nanocluster solutions (from left to right) under long-wavelength UV lamp irradiation (366 nm). The leftmost solution appears slightly bluer, but similar in color to Au_8 (center) [14] due to the color sensitivity of the human eye. Green emission appears weaker due to inefficient excitation at 366 nm.

from redissolved Au-nanodot powders have identical properties to those initially created.

The dependence of emission energy on the number of atoms, N , in each gold nanocluster (Fig. 3) is quantitatively fit for the smallest nanoclusters with no adjustable parameters by the simple scaling relation of $E_{\text{Fermi}}/N^{1/3}$, in which E_{Fermi} is the Fermi energy of bulk gold [3,18,19]. Identical to that for gas phase alkali metal nanocluster

electronic absorptions [5,20] the transition energy scaling with inverse cluster radius indicates that electronic structure is solely determined by the Au nanocluster free-electron density and nanocluster size. Previously

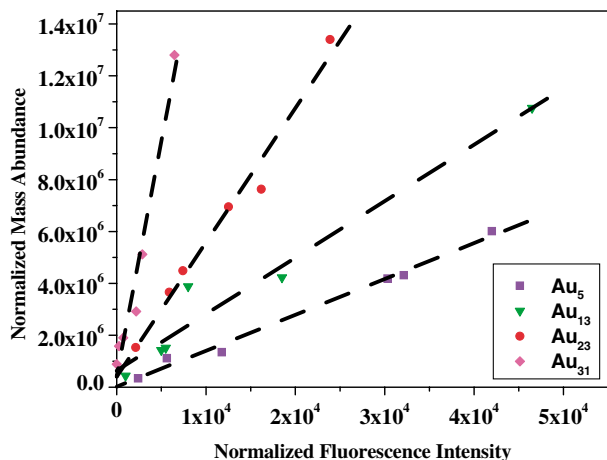


FIG. 2 (color online). Fluorescent nanocluster size determinations. In addition to separately identified Au_8 (455 nm) [14], nanocluster sizes (emission maxima) were determined to be Au_5 (385 nm), Au_{13} (510 nm), Au_{23} (760 nm), and Au_{31} (866 nm) through linear correlation of mass abundance and fluorescence intensity at each emission maximum. The mass abundances of all gold nanocluster solutions were measured by electrospray ionization (ESI) mass spectrometry with identical ionization conditions. The reproducible and gentle ionization procedure yielded only one mass species linear in emission intensity for each emission maximum. This one-to-one correspondence between mass abundance and fluorescence enabled unambiguous assignments of fluorescent gold nanocluster sizes.

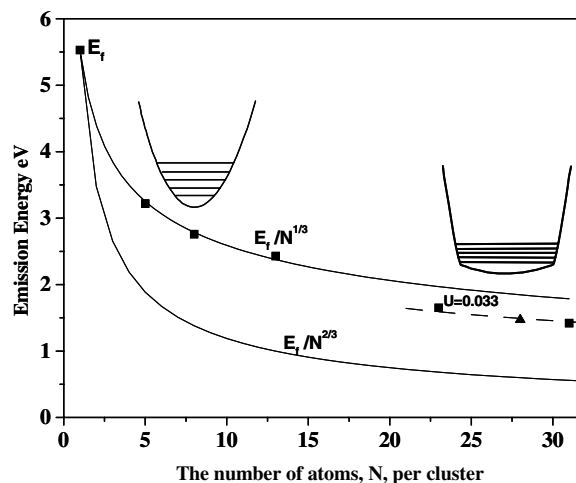


FIG. 3. Correlation of the number of atoms, N , per cluster with emission energy. Emission energy decreases with increasing number of atoms. The correlation of emission energy with N is quantitatively fit with $E_{\text{Fermi}}/N^{1/3}$, as predicted by the spherical jellium model [2,4]. Emission energies of Au_{23} and Au_{31} exhibit slight deviations from the $E_{\text{Fermi}}/N^{1/3}$ scaling. Consistent with the narrow excitation and emission spectra, the potential confining the free electrons flattens slightly for Au_{23} and Au_{31} , with an anharmonicity of $U = 0.033$. The one-electron artificial atom (Bohr model) scaling ($N^{-2/3}$) of semiconductor quantum dots (scaled to the metallic limit of the Fermi energy) is also shown to delineate the different scaling laws of quantum-confined metals and semiconductors. Other measurements of Au_{28} [6] emission (\blacktriangle) and the measured (nonfluorescent) transition energies of Au_{11} [22] and Au_{20} [21] are all consistent with the observed scaling relations.

observed only in gas phase absorption spectra of alkali metals, the free-electron shell-filling model corresponds exactly to the spherical jellium approximation—the simplest model for explaining delocalized, free conduction electron behavior relative to the atomic cluster core, and an excellent basic model explaining plasmon absorption in large nanoparticles [3,18,19]. These quantum-confined protoplasmonic transitions of the free conduction electrons suggest nearly spherical nanocluster electronic structures with electrons bound by an approximately harmonic potential in three dimensions. While a harmonic potential would give a R^{-2} electronic transition energy dependence, the degeneracy in filling the delocalized nanocluster energy level shells ($1s$, $1p$, $1d$, $2s$, $1f$, $2p$, ...) and the size-independent electron density for the given material yield an effective R^{-1} dependence on cluster size [2,3], further demonstrating the metallic origin of these Au nanocluster fluorescent transitions.

At larger nanocluster sizes ($N = 23$ and 31), electron screening increases and the potential bounding each electron flattens, thereby slightly increasing the anharmonicity. Figure 3 shows that the potential confining free electrons in larger gold clusters Au_{23} and Au_{31} flattens only slightly [3,18]. Even the highest occupied to lowest unoccupied molecular orbital gaps in gas phase Au_{20} [21] and in water-soluble Au_{11} [22] and Au_{28} [6] lie close to the same curve and are consistent with our results (Fig. 3). While only magic cluster sizes correspond to shell closings [18], the approximately spherical electronic structure indicated by the linear scaling with inverse cluster radius shows that these nanomaterials are “multielectron artificial atoms” [2,23]. This artificial atom behavior results from the conduction electrons making intraband transitions between nanocluster electronic states of well-defined angular momenta, thereby leading to discrete excitation and emission spectra. The primary difference between these and true atoms is that the electron density does not change in the clusters, while it does as atomic number increases [2,3]. Consequently, in contrast to predictions of planarity for gas phase $\text{Au}_{N \leq 7}$ nanoclusters [24], the PAMAM-encapsulated nanocluster geometries must be approximately spherical to yield the observed scaling.

The detailed photophysical properties of different water-soluble gold nanoclusters (Table I) indicate that these Au nanodots behave as quantum-confined, size-tunable fluorophores. The high quantum yields are comparable to the best water-soluble emitters currently available, ranging from 70% for UV-emitting Au_5 to $\sim 10\%$ for Au_{31} in the near IR. The decreasing quantum yields with decreasing energy are consistent with increased nonradiative pathways at lower energies (i.e., the “energy gap law”) [25]. Dividing the measured lifetime (Table I) by the fluorescence quantum yield gives the intrinsic lifetimes, which increase monotonically with decreasing energy as expected for spontaneous emission. In contrast to larger semiconductor nanocrystals [15,23], dendrimer

TABLE I. Measured Au-nanodot photophysical properties.

Gold cluster	Excitation (FWHM) (eV)	Emission (FWHM) (eV)	Quantum yield (%)	Lifetime (ns)
Au_5	3.76 (0.42)	3.22 (0.45)	70	3.5
Au_8	3.22 (0.54)	2.72 (0.55)	42	7.5
Au_{13}	2.86 (0.38)	2.43 (0.41)	25	5.2
Au_{23}	1.85 (0.21)	1.65 (0.26)	15	3.6
Au_{31}	1.62 (0.20)	1.41 (0.10)	10	

encapsulated gold nanodots have very well-defined excitation and emission spectra while requiring neither complicated high temperature syntheses with toxic precursors nor difficult overcoating with surface passivation and solubilization chemistry [26] for applicability as bio-labels. The much narrower emission and smaller Stokes shifts at larger nanocluster sizes (e.g., Au_{23} and Au_{31}) indicate less distortion in the excited state than in the smaller nanoclusters. Such well-defined, tunable discrete excitation and emission suggest that these nanomaterials may find utility as energy transfer pairs, a task for which semiconductor quantum dots are ill-suited because of their extremely broad excitation spectra and larger fluorophore size.

As these nanoclusters are too small to have the continuous density of states and plasmon absorptions characteristic of larger nanoparticles (>2 nm) [13,27] the transition energy instead of the plasmon absorption width scales with inverse cluster radius [1–3,28]. The size-dependent scaling of excitation and emission energies with $E_{\text{Fermi}}/N^{1/3}$ directly indicates that free-electron behavior begins in Au_N as small as $N = 5$. Such free-electron protoplasmonic intraband absorption and fluorescence give rise to discrete size-dependent Au transitions throughout the visible beginning at the few-atom size scale. As nanocluster size increases further, transition energies decrease with the increasing density of states, thereby forcing energy level spacings to eventually become comparable to available thermal energy. This relaxes the angular momentum selection rules as single-electron states become less well-defined in favor of the effectively continuous density of states characteristic of plasmon absorption within nanoparticles and bulk metals. Consequently, by directly probing the lowest energy absorptions and emissions, these studies connect the seemingly disparate nanocluster transition energies and plasmon absorption widths, both of which scale with inverse particle radius (R^{-1} or, equivalently, $N^{-1/3}$) [29]. With increasing size and decreasing transition energy, confinement switches from being relative to the Fermi wavelength (yielding discrete size-dependent optical transitions) to being relative to the electron mean free path (yielding plasmon widths that scale with the free-electron DOS and the imaginary dielectric constant). Both regimes scale with inverse cluster radius as the delocalized free-electron states giving rise to nanocluster

fluorescence become sufficiently dense at larger sizes to enable Au nanoparticle plasmon absorptions with characteristic $N^{-1/3}$ scalings of the plasmon width [29]. Consequently, the size-dependent transition frequencies of our water-soluble Au nanoclusters are the small size limit of the plasmon absorption within bulk metals and provide a smooth connection between atomic and metallic behavior with true protoplasmonic fluorescence that is well described at all sizes by the spherical jellium model.

In conclusion, we have created novel, highly fluorescent, water-soluble quantum dots from PAMAM-encapsulated Au that behave as multielectron artificial atoms with size-tunable, discrete electronic transitions between states of well-defined angular momenta. Correlations of Au nanocluster sizes with transition energies are well fit with the simple relation, $E_{\text{Fermi}}/N^{1/3}$, indicating protoplasmonic fluorescence corresponding to the jellium model. Thus, the intraband transitions are the low number limit of the plasmon before the onset of collective dipole oscillations that occur when a continuous density of states is reached. Providing the “missing link” between atomic and nanoparticle behavior in noble metals, these highly fluorescent, water-soluble Au nanoclusters offer complementary transition energy size scalings at smaller dimensions than do semiconductor quantum dots. The unique discrete excitation and emission coupled with facile creation in aqueous solution open new opportunities for noble metal nanoclusters as biological labels, energy transfer pairs, and other light emitting sources in nanoscale electronics.

The authors appreciate exciting discussions with R. L. Whetten, W. A. de Heer, and L. M. Tolbert. Financial support from NSF (BES-0323453), NIH (1R01GM068732), the Sloan and Dreyfus Foundations, the Blanchard and Vassar Woolley endowments, and the Center for Advanced Research in Optical Microscopy at Georgia Tech are gratefully acknowledged.

*To whom correspondence should be addressed.

Email address: dickson@chemistry.gatech.edu

- [1] N. Nilius, T. M. Wallis, and W. Ho, *Science* **297**, 1853 (2002).
- [2] H. Haberland, *Clusters of Atoms and Molecules* (Springer-Verlag, Berlin, 1994).
- [3] W. A. de Heer, *Rev. Mod. Phys.* **65**, 611 (1993).
- [4] U. Kreibitz and M. Vollmer, *Optical Properties of Metal Clusters* (Springer-Verlag, Berlin, 1995).
- [5] T. Reiners *et al.*, *Phys. Rev. Lett.* **74**, 1558 (1995).
- [6] S. Link *et al.*, *J. Phys. Chem. B* **106**, 3410 (2002).
- [7] L. A. Peyser *et al.*, *Science* **291**, 103 (2001).
- [8] L. König *et al.*, *Science* **274**, 1353 (1996).
- [9] B. Palpant *et al.*, *Phys. Rev. B* **57**, 1963 (1998).
- [10] J. P. Wilcoxon *et al.*, *J. Chem. Phys.* **108**, 9137 (1998).
- [11] T. Huang and R. W. Murray, *J. Phys. Chem. B* **107**, 7434 (2003).

- [12] T. Huang and R. W. Murray, *J. Phys. Chem. B* **105**, 12 498 (2001).
- [13] J. M. J. Frechet, *Science* **263**, 1710 (1994).
- [14] J. Zheng, J. T. Petty, and R. M. Dickson, *J. Am. Chem. Soc.* **125**, 7780 (2003).
- [15] L. E. Brus, *J. Chem. Phys.* **80**, 4403 (1984).
- [16] All clusters are readily created in both 2nd and 4th generation hydroxyl- and amine-terminated PAMAM. To synthesize gold nanoclusters, the general procedure consists of codissolving G4-OH or G2-OH and $\text{HAuCl}_4 \cdot n\text{H}_2\text{O}$ (Aldrich) into 2 ml of distilled water (18 M Ω). Gold ions were reduced by slowly adding an equivalent of NaBH_4 into solution. Small fluorescent Au nanodots (i.e., PAMAM-encapsulated nanoclusters) and large nanoparticles are simultaneously created. Solutions are stirred for two days at room temperature until reaction and aggregation processes are complete. Solutions are subsequently purified through centrifugation (16000 g) to remove the large gold nanoparticles, leaving clear, fluorescent Au-nanodot solutions. Au nanocluster excitation and emission colors are affected by dendrimer generation, gold salt, and dendrimer concentrations. UV-emitting Au_5 is preferentially created in 0.5 μmol G4-OH and 0.5 μmol HAuCl_4 in distilled water. Blue emitting Au_8 synthesis has been reported recently [10]. Green-emitting Au_{13} is synthesized with 0.51 μmol G2-OH and 3 μmol HAuCl_4 in 2 ml distilled water. High concentrations of Au_{23} and Au_{31} were synthesized with 6.0 and 7.5 μmol HAuCl_4 , respectively, codissolved into 2 ml with 0.5 μmol G4-OH. All nanoclusters can be created with AuBr_3 as well.
- [17] L. Balogh and D. A. Tomalia, *J. Am. Chem. Soc.* **120**, 7355 (1998).
- [18] K. Clemenger, *Phys. Rev. B* **32**, 1359 (1985).
- [19] W. D. Knight *et al.*, *Phys. Rev. Lett.* **52**, 2141 (1984).
- [20] W. A. de Heer *et al.*, *Phys. Rev. Lett.* **59**, 1805 (1987).
- [21] J. Li *et al.*, *Science* **299**, 864 (2003).
- [22] P. A. Bartlett, B. Bauer, and S. J. Singer, *J. Am. Chem. Soc.* **100**, 5085 (1978).
- [23] A. P. Alivisatos, *Science* **271**, 933 (1996).
- [24] H. Hakkinen and U. Landman, *Phys. Rev. B* **62**, 2287(R) (2000).
- [25] J. Michl and V. Bonacic-Koutecky, *Electronic Aspects of Organic Photochemistry* (John Wiley & Sons, Inc., New York, 1990).
- [26] B. Dubertret *et al.*, *Science* **298**, 1759 (2002).
- [27] Y. G. Kim, S. K. Oh, and R. M. Crooks, *Chem. Mater.* **16**, 167 (2004).
- [28] O. C. Thomas *et al.*, *Phys. Rev. Lett.* **89**, 213403 (2002).
- [29] Absorption is governed by $k(N)$, the size-dependent imaginary part of the refractive index, $n'(N) = n(N) + ik(N)$, while plasmon width results from the imaginary portion of the dielectric constant, $\epsilon(N) = \epsilon_1(N) + i\epsilon_2(N)$. Because $\epsilon(N) = n'(N)^2$ for nonmagnetic materials, $\epsilon(N) = [n(N)]^2 - [k(N)]^2 + 2in(N)k(N)$ and the portion governing the plasmon width is simply $\epsilon_2(N) = 2n(N)k(N)$, and is linearly dependent on $k(N)$. Therefore, any size dependence in absorption is directly related to the imaginary portion of the dielectric constant which governs plasmon width, thereby connecting the atomic and nanoparticle limits.